JOURNAL OF MATERIALS SCIENCE 27 (1992) 1546–1552

Effect of hydrothermal and thermal treatments on the physicochemical properties of Mg–Al hydrotalcite-like materials

F. M. LABAJOS, V. RIVES*
Dipartamento de Química Inorgánica, Universidad de Salamanca, Facultad de Farmacia, Salamanca, Spain

M. A. ULIBARRI
Dipartamento de Química Inorgánica e Ingeniería Química, Universidad de Córdoba, Facultad de Ciencias, Córdoba, Spain

The synthesis and characterization of hydrotalcite-like materials is described. As the time to which the samples have been submitted to a hydrothermal treatment is prolonged, a change in the Mg/Al ratio is observed, together with a more ordered structure of the species existing in the interlayer space. Calcination at increasing temperatures leads to decomposition of this compound, with the final formation of MgO and $MgAl_2O_4$. Changes taking place during these processes have been related to the decrease observed in the specific surface area of the samples upon prolonging the hydrothermal treatment, as well as its development and further decrease upon thermal treatment.

1. Introduction

The existence of layered double hydroxides (LDH) has been known since the 1930s, when these materials were synthetized by Feitknecht [1, 2] through reaction between dilute solutions of metal ions with bases, leading, upon ageing, to hydrotalcite-like (HT) materials; some other preparation methods have been recently reviewed by Reichle [3]. Nowadays, they are recognized as compounds with general formula $[M_{1-x}M'_x(OH)_2]^{x+}X_{x/m}\cdot nH_2O$, where M = Mg(II), Zn(II), Ni(II), . . . , M′ = Al(III), Fe(III), . . . and $X = CO_3^{2-}$, NO_3^-, SO_4^{2-}, ... Their structure consists of positively charged brucite-like layers, $[MM'(OH)_2]$, with the interlayer space filled with anions and water molecules. Actually, LDH are the only known layered materials with positively-charged layers [4], and, as smectites, they exhibit swelling properties and the interlayer space can be modified by intercalation of other anions. As zeolites, these materials exhibit molecular sieve properties, thus absorbing nitrogen, oxygen and CO_2, but not hydrogen [5]. In addition to its academic interest, the recent growth in research in this area mainly comes from the use of Ni-containing HT-like materials as catalysts [6, 7], hydrotalcite itself for propiolactone polymerization [8], and aldol condensation in the gas phase after thermal activation [3, 9] of samples containing first-series transition cations in the brucite-like layers. They have been also used for propene oligomerization [10]. Suzuki *et al.* [11, 12] have reported halide-exchange reactions using HT-like materials. On the other hand, several authors have reported the exchange of the anions existing in the interlayer space with surfactants, thus allowing an accurate determination of the size of these molecules [13, 14]. Another field where the use of LDH is currently investigated is the introduction of polynuclear anions in the interlayer space and subsequent reaction to yield pillared materials [15].

As reported, some of the applications of LDH materials depend on the nature of the cations existing in the brucite-like layers, others depend on the nature of the interlayer anion, and in some other cases the material is partially or totally decomposed to yield new ones with specific properties (usually as catalysts). The aim of the present work is to obtain insight into the nature of LDH materials when the experimental conditions during hydrothermal or thermal treatment are changed.

2. Experimental procedure

2.1. Sample preparation

The samples were obtained by dropwise adding, at room temperature, a solution containing 0.5 mol $MgCl_2\cdot 6H_2O$ and 0.25 mol $AlCl_3\cdot 6H_2O$ dissolved in 250 ml of bidistilled water to a vigorously stirred solution (500 ml) containing 1.7 mol NaOH and 0.5 mol Na_2CO_3 (the so-called "constant pH" method). The resulting heavy suspension was further stirred at room temperature for 2 h, and then the solvent was very slowly evaporated (ca. one week) at 325 K in a water bath. Four samples were therein

* To whom all correspondence should be addressed.

0022–2461

obtained: sample 0 was aged at room temperature for 2 weeks, while samples I, II and III were aged hydrothermally for 4, 8 and 13 days, respectively, at 400 K in a stainless steel Phaxe 2001 bomb. The solids were washed until the absence of chloride and sodium ions was confirmed in the washing liquids by conventional analytical methods. Chemicals were from Probus or Panreac, with adequate quality.

2.2. Measurements

Instrumental facilities were as follows: (i) chemical analysis for Mg and Al was performed by atomic absorption (ELL-240); (ii) X-ray diffraction (XRD) profiles were recorded on a Philips PW-1070 or a Siemens D-500 instrument, using Ni-filtered CuK_α radiation ($\lambda = 154.05$ pm); (iii) differential thermal analysis (DTA) and thermogravimetric analysis (TG) were performed in DTA-1700 and TGS-2 instruments, from Perkin-Elmer, coupled to a Perkin-Elmer 3600 Data Station, using a heating rate of 10 K min^{-1} in air; (iv) Fourier-transformed infrared (FT-IR) spectra were recorded by the KBr pellet technique in a Perkin-Elmer FT-IR 1730 instrument, with a nominal resolution of 2 cm^{-1} and averaging 100 scans; (v) transmission electron micrographs were obtained on a Jeol 200CX microscope; and (vi) specific surface area measurements were carried out in a Micromeritics Flowsorb II 2300 instrument, using an He/N_2 (30:70) mixture from Sociedad Castellana del Oxigeno (Spain); in some cases, full adsorption/desorption isotherms were measured in a conventional Pyrex high-vaccum system equipped with an MKS pressure transducer, grease-free stopcocks, an APV-DD4 rotatory pump and a silicon oil diffusion pump.

3. Results and discussion

3.1. Hydrothermally treated samples

The results of the chemical analysis for all samples are included in Table I. From the Mg(II) and Al(III) content, and assuming (as shown by other techniques, see below) that the samples have attained a layered, hydrotalcite-like structure, the carbonate content has been calculated. As the hydrothermal treatment is prolonged, the Mg:Al ratio slightly increases. In all cases, this Mg:Al ratio is within the maximum stability range, as reported by Brindley and Kikkawa [16].

The X-ray diffraction patterns of all four samples undoubtedly demonstrates its layered structure; peaks due to diffraction by the (0 0 l) planes are enhanced when the profiles are recorded by the oriented aggregate technique. The sharpness of the peaks increases as the hydrothermal treatment is prolonged, indicating an improved crystallinity. As an example, the $31° \leqslant 2\theta \leqslant 37°$ range for all four samples is shown in Fig. 1, where it can be seen that those peaks due to diffraction by planes (0 1 2) and (0 0 9) are better resolved in samples hydrothermally treated than in the sample aged at room temperature (sample 0).

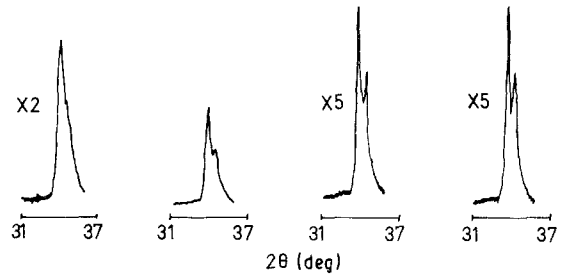

Figure 1 X-ray diffraction profiles (left to right) of samples 0, I, II and III (range $31° \leqslant 2\theta \leqslant 37°$).

All four samples behaved similarly during the thermal study. The results for sample III are shown in Fig. 2. The DTA profile shows an intense endothermic peak close to 530 K, together with two weaker energy absorptions at 613 and 712 K. These positions are nearly the same for samples I and II, although for sample 0 the energy absorption at 613 K is merely a shoulder of the absorption at higher temperature. In addition, the position of the peak close to 712 K gradually shifts from 687 K for sample 0 to 712 K for sample III. The position of the first peak coincides with the first weight loss recorded in the TG diagram between 300 and 550 K, which represents ca. 19% of the original weight for sample 0 and 13–14% for samples I, II and III. The other DTA peaks should be ascribed to the weight loss recorded between 550 and 1100 K as two overlapped steps, although these steps are badly resolved for sample 0. The very first weight loss should be ascribed to elimination of water molecules from the interlayer space, as recorded at fairly low temperatures, while the remaining peaks should originate from removal of carbonate ions as CO_2, and hydroxyl groups from the layered structure as water;

TABLE I Empirical formulae and specific surface area values[a]

Sample	Mg	Al	OH	CO_3^{2-}	H_2O	Mg/Al	SSA
0	0.65	0.35	2	0.17	0.88	1.89	115
I	0.69	0.31	2	0.16	0.66	2.21	35
II	0.70	0.30	2	0.15	0.57	2.31	21
III	0.72	0.28	2	0.14	0.61	2.54	22

[a] Results for Mg and Al from chemical analysis; water content from TG. SSA values in m^2 g^{-1}.

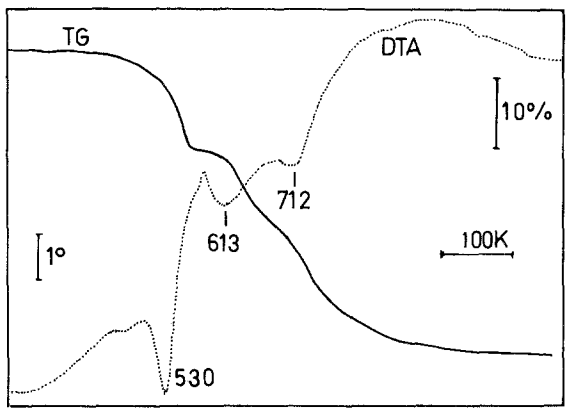

Figure 2 DTA and TG profiles of sample III, recorded in air (heating rate 10 K min^{-1}).

however, we could not analyse the gases evolved during thermal decomposition and thus we could not determine whether one peak corresponds to removal of CO_2 and the other to removal of water, or, alternatively, whether both processes contribute to both peaks. From the weight losses corresponding to the first step, the water content of the samples has been calculated, the values obtained being included in Table I. As can be observed in this table, the amount of molecular water retained in the interlayer space is larger in the non-treated sample than in those treated hydrothermally. With regards to the second and third endothermic peaks, responsible for the two overlapped weight losses above 550 K, it is difficult to ascertain their origin. A simple calculation, however, can be made: these two endothermic DTA peaks join at 683 K, and the weight loss from 550 K (i.e. once the water molecules have been removed) up to 683 K represents 11.9% of the original weight of the sample; removal of carbonate ions as CO_2 represents only 8%, and removal of hydroxyl groups as water molecules 22.9%. Thus, although CO_3^{2-} species should probably be removed from the interlayer space before hydroxyl groups are removed from the brucite-like layers, these begin to be removed just before elimination of carbonate is completed. This result is, however, interesting, as it indicates that the layered structure can be preserved even after calcination to withdraw interlayer anions.

The FT-IR spectrum of sample 0 is shown in Fig. 3. Those for the treated samples are essentially similar, and the differences found will be discussed later. The strong absorption at 3441 cm^{-1} is due to the ν_{OH} mode of free and hydrogen-bonded hydroxyl groups and water molecules, whose bending mode is responsible for the medium-intensity band at 1630 cm^{-1}. The split band with maxima at 1400 and 1364 cm^{-1} should be ascribed to the ν_3 mode (antisymmetric stretching) of CO_3^{2-} species, recorded as a single band (E′ symmetry) at 1450 cm^{-1} for free CO_3^{2-} species, but which splits because of the lower symmetry in the interlayer space, probably due to hydrogen bonding with OH groups and/or H_2O molecules. The values found here for the position of this split band are very close to those reported by Hernández-Moreno *et al.* [17] for Al,Li-hydrotalcite materials. The low crystallinity of sample 0, and the consequent disordered structure of the interlayer space, would give rise in addition to activation of the ν_1 mode (symmetric stretching) of CO_3^{2-} species, originally forbidden in IR, thus accounting for the very weak absorption at 1060 cm^{-1}. This band is even weaker and hardly recorded in the spectra of samples I, II and III, probably due to their better crystallization and higher degree of order. Bands ν_2 (out-of-plane deformation) and ν_4 (in-plane bending) of carbonate species are also recorded at 874 and 671 cm^{-1}, respectively. The shoulder at 950 cm^{-1} has been ascribed to the presence of hydroxyl groups [17], while other bands in the 800–250 cm^{-1} range are due to lattice vibrations, mainly involving translational motions of oxygen ions in the layers.

A detailed study of the differences in the spectra of the samples studied, with regard to the ν_{OH} mode close to 3500–3400 cm^{-1}, and the ν_3 (CO_3^{2-}) mode close to 1400–1300 cm^{-1}, is summarized in Figs 4 and 5. As mentioned above, the ν_3 mode of CO_3^{2-} species should be recorded as a single peak if this moiety preserves its D_{3h} symmetry, but should split upon deformation, usually by bonding through one or two of its oxygen

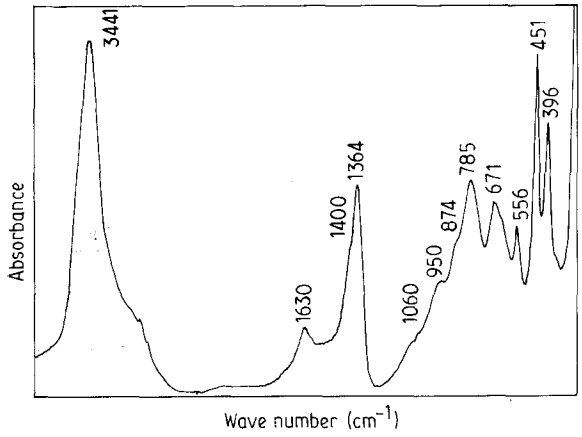

Figure 3 FT-IR spectrum of sample 0.

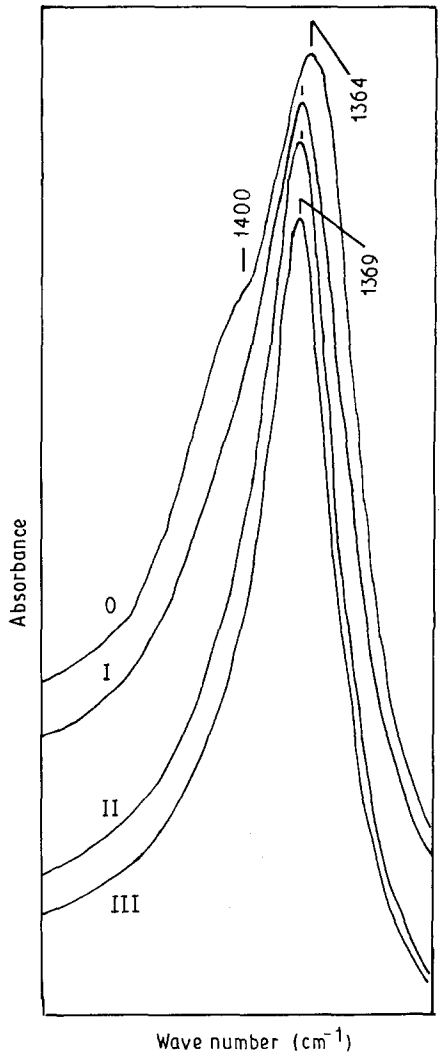

Figure 4 FT-IR spectra of samples 0, I, II and III in the ν_{OH} region.

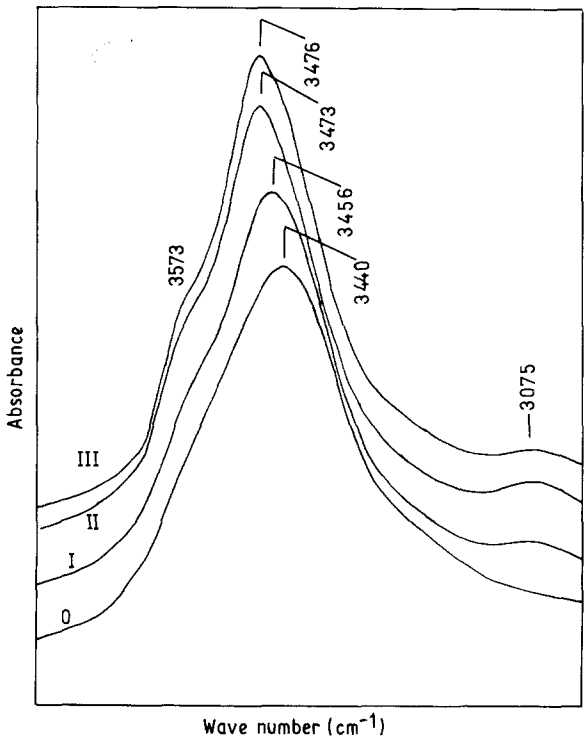

Figure 5 FT-IR spectra of samples 0, I, II and III in the ν_3 (CO_3^{2-}) region.

atoms, then decreasing the symmetry to C_{2v}. Unfortunately, both situations (linking through one or two oxygen atoms) give rise to such a C_{2v} symmetry, and thus it cannot be ascertained, from the analysis of the number of bands, which type of linkage actually exists. Nevertheless, the results depicted in Fig. 4 show that such splitting is highly evident for sample 0, where an absorption band at 1364 cm^{-1}, with a prominent shoulder at 1400 cm^{-1}, is recorded, thus indicating a high degree of disorder in the interlayer space of this sample. However, the samples hydrothermally treated show a single band (although wider in the high wave-number tail for sample I) centred in all cases at 1369 cm^{-1}, indicating that, at least in samples II and III, the CO_3^{2-} species have attained a highly symmetric geometry. However, this value is very much lower than that reported [18] for free CO_3^{2-} species, 1415 cm^{-1}, indicating a large electrostatic interaction between the hydroxyl groups and the carbonate species, which should then be located in the interlayer space with its symmetry plane parallel to the layers, thus accounting for the maintained D_{3h} symmetry.

With regard to the data reported in Fig. 5 for the ν_{OH} mode, some differences can be also observed in the behaviour of the different samples. The position of the maximum shifts towards larger wave-numbers as the sample is hydrothermally treated, from 3440 cm^{-1} for sample 0 to 3476 cm^{-1} for sample III, whose spectrum clearly shows a shoulder at 3573 cm^{-1} and the arising of an absorption band at 3075 cm^{-1}. The position of this absorption band at ca. 3500 cm^{-1} should be controlled by the cation to which the hydroxyl group is bonded, and if different types of M–OH moieties exist, the band should be wider or should split. The spectrum for pure brucite shows a sharp absorption at 3705 cm^{-1} with a weak and wider band at 3650 cm^{-1} [19]. The spectrum of $Al(OH)_3$ shows a more complicated feature, with sharp, intense bands at 3630 and 3525 cm^{-1}, a wide, medium band at 3450 cm^{-1} and two weaker bands, also wide at 3395 and 3320 cm^{-1}. The shift towards lower wave numbers in $Al(OH)_3$ and in our samples should be due to a lower electron density of the O–H bond in hydroxyl groups bonded to Al(III) cations, because of the larger polarizing effect of the Al^{3+} cation. Actually, as the aluminium content decreases (from sample 0 to sample III), the band shifts towards larger wave numbers. The development of the shoulder at 3573 cm^{-1} upon hydrothermal treatment should be ascribed to a "better defined" structure of the OH groups because of the improved crystallinity of the samples. With respect to the band at 3075 cm^{-1}, it has been ascribed to water molecules hydrogen-bonded to carbonate ions in the interlayer [6, 20]. If Figs 4 and 5 are compared, it is observed that the band at 3075 cm^{-1} develops clearly in sample III, whose ν_3 (CO_3^{2-}) band is sharp and single; so it is quite surprising that formation of water–carbonate linkages (thus accounting for this band at 3075 cm^{-1}) is evident in the sample where the CO_3^{2-} moiety seems to attain a more symmetric structure. Nevertheless, we suspect that such ascription seems to be true if we assume that the higher crystallinity of sample III gives rise to a more ordered structure not only in the layers, but also in the interlayer space, thus giving rise to a more symmetric interaction between carbonate ions and water molecules: if carbonate ions have their plane parallel to that of the layers, and interact simultaneously with three water molecules, the D_{3h} symmetry is retained, thus accounting for the single band at 1369 cm^{-1}. A different situation should exist in sample 0, where the poor crystallinity gives rise to a more disordered structure, giving rise to CO_3^{2-} species in C_{2v} symmetry, thus accounting for the split ν_3 mode at 1400 and 1364 cm^{-1}, the interaction with water molecules being non-specific, and thus accounting for the badly resolved absorption at 3075 cm^{-1}. The situation in samples I and II should be more or less between those for samples 0 and III.

The values for the specific surface area (SSA) of the samples are included in Table I. Sample 0 has a very large SSA, decreasing in sample I and further decreasing for samples II and III, although in these two latter cases the value is the same within experimental error. All nitrogen adsorption isotherms correspond to type II in the IUPAC classification, originating from adsorption on non-porous or mesopore samples [21]. The changes observed cannot be due to the different aluminium contents, as these vary very much less than is observed for the SSA values, and thus a sintering of crystallites during the hydrothermal treatment seems to take place. Actually, this is the conclusion reached from the analysis of the transmission electron micrographs in Fig. 6. Sample 0 (Fig. 6a) appears as very small particles, the size increasing in sample I (Fig. 6b), where they can be seen as stacks of lamellar hexagonal particles with an average size close to 60–70 nm. This increase is clearly greater for samples II and III (Fig.

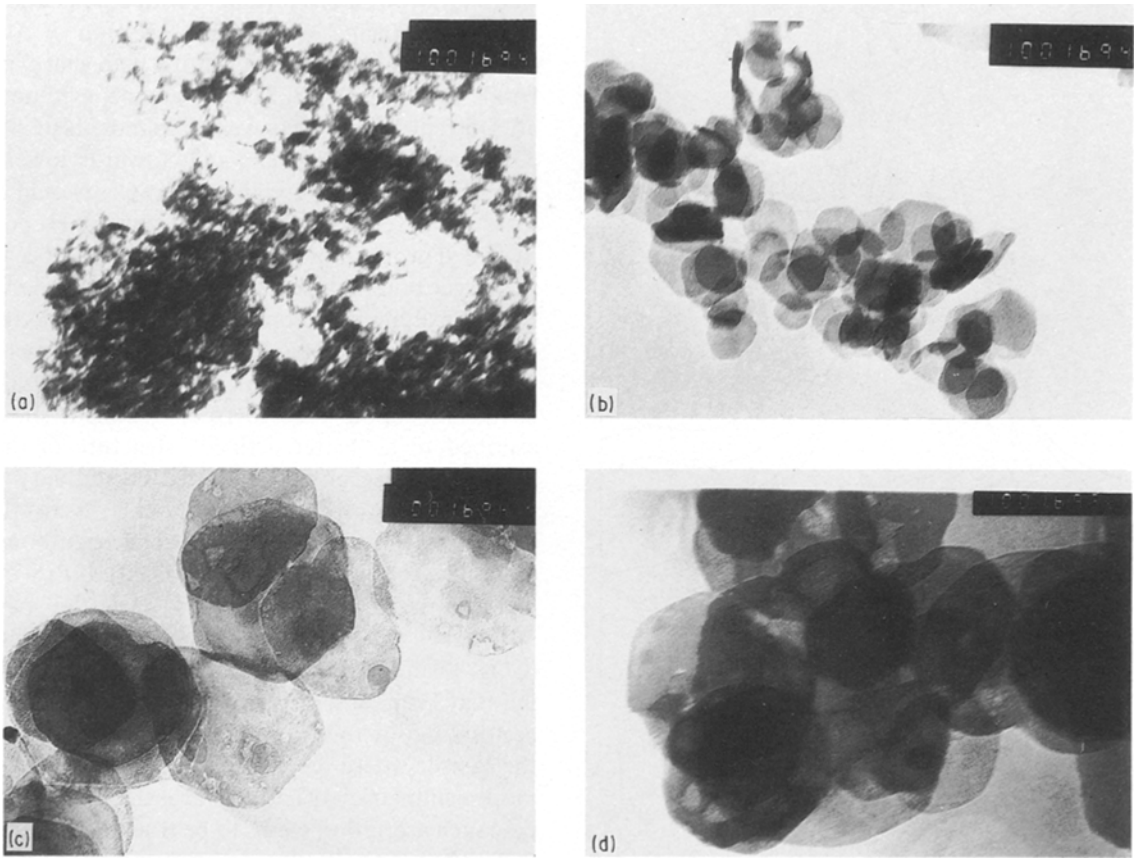

Figure 6 Transmission electron micrographs of samples (a) 0, (b) I, (c) II and (d) III (× 70 000).

6c and d), where hexagonal particles with a size larger than 100 nm are seen. These results, together with those from nitrogen adsorption, indicate that the hydrothermal treatment has led to sintering and crystallization of the samples, thus accounting for the higher degree of symmetry in the samples hydrothermally treated, as suggested by the FT-IR results above.

The differences in the morphology of the samples also give rise to differences in the way nitrogen is adsorbed. In Fig. 7, the so-called t-plots corresponding to the amount of gas adsorbed versus the thickness of the adsorbed layer, for all four samples, are included. Linear plots passing through the origin should be obtained for multilayer adsorption in the absence of any condensation into pores, as reported in this work for samples hydrothermally treated. However, the upward deviation for sample 0 reflects the increased uptake due to condensation in larger pores, probably interparticle pores, as the interlayer space in all samples is filled with water molecules and carbonate anions that are not removed by the gentle outgassing treatment prior to nitrogen adsorption runs. The fact that in all cases straight lines passing through the origin are obtained indicates that micropores do not develop in these samples.

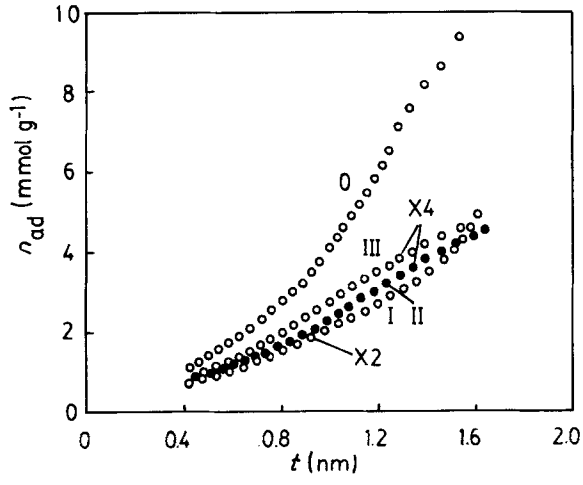

Figure 7 t-plots for samples 0, I, II and III.

3.2. Thermally treated samples

As mentioned above, thermal treatment of the sample leads to removal of water molecules, interlayer anions and hydroxyl groups from the brucite-like layers. So, it is quite interesting to analyse changes taking place in the structure of the solid as the calcination temperature is increased, in order to assess the formation of new crystalline phases, as well as their surface properties. In the present study, sample 0 was submitted to calcination in air for 2 h at 400, 548, 773, 1023, 1273, and 1373 K, that is, temperatures below and above the features recorded in the DTA curve. The samples thus obtained were studied by XRD, TEM and specific surface area monitoring.

The XRD profiles are shown in Fig. 8. From the fairly crystalline material obtained upon calcination at 400 K, where lines due to the layered hydrotalcite-like material are recorded, calcination at 548 K, that is,

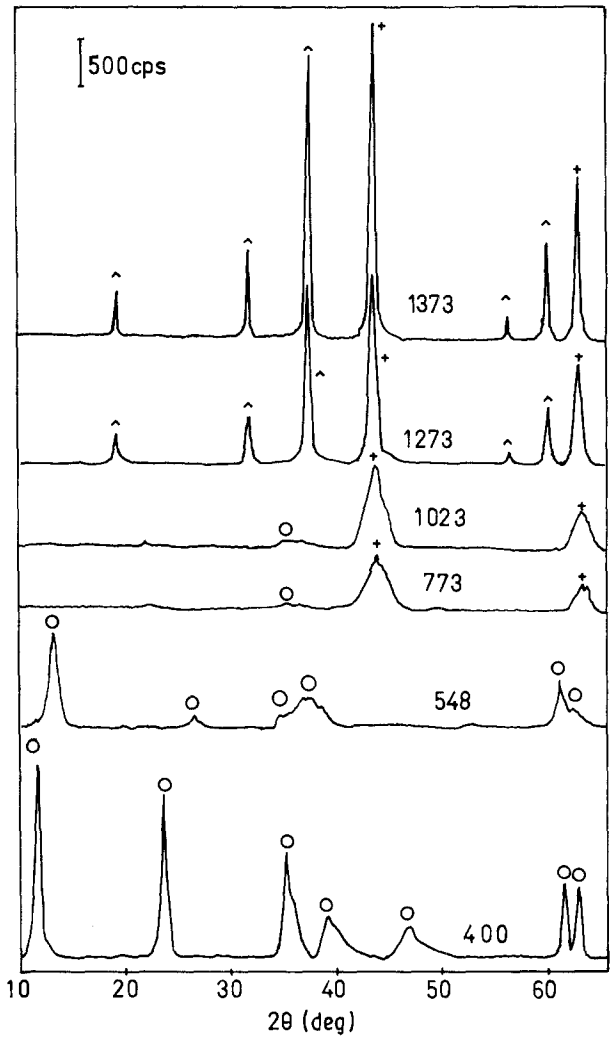

Figure 8 XRD profiles of sample 0 submitted to calcination in air for 2 h at the indicated temperatures: (∧) $MgAl_2O_4$, (+) MgO, (○) HT.

after the first DTA endothermic peak due to removal of the interlayer water molecules, gives rise to lines shifted towards higher 2θ values. The peak close to ca. 2θ = 12° and that at 2θ = 26° should originate from the same planes that give rise to peaks at 2θ = 12 and 23° in sample calcined at 400 K, the lower interlayer spacings originating from a decrease in the interlayer space because of removal of water molecules. Other peaks are ill-defined, due to a poorer crystallinity of the solid. Calcination at 773 K, a temperature slightly above the main weight loss recorded in the TG curve (Fig. 2) responsible for the energy-absorption DTA peaks at 613 and 712 K, gives rise to a highly amorphous material, with main diffraction peaks close to 2θ = 45 and 62° which may be due to crystallization of MgO, although the last peak may also be residual of the two peaks slightly above 2θ = 60° due to hydrotalcite; moreover, a very weak peak at 2θ = 35° should be ascribed to hydrotalcite. The other calcination temperatures were chosen in order to analyse the crystallization of other products. So, calcination at 1023 K only produces minor changes in the XRD profiles. In contrast, upon calcination at 1273 and 1373 K (the maximum temperature attainable by our experimental techniques) gives rise

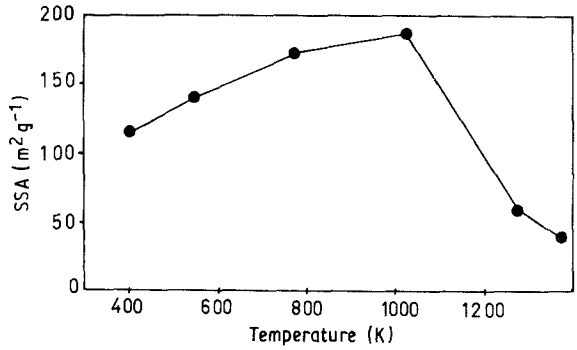

Figure 9 Change in the specific surface area of sample 0 after calcination in air for 2 h at the indicated temperatures.

to the appearance and sharpening of diffraction peaks that are due to MgO and $MgAl_2O_4$, with the expected spinel structure. According to the formula of the starting sample (sample 0) with an Mg/Al ratio of 1.89, formation of MgO, in addition to that of spinel (Mg/Al = 0.5), should be expected.

Decomposition of the solid up to 1023 K (i.e. up to formation of the amorphous material) gives rise to a development of the specific surface area up to values close to 200 $m^2 g^{-1}$ (Fig. 9), but crystallization of MgO and $MgAl_2O_4$ leads to a sintering of the material, finally producing a solid with a specific surface area of ca. 50 $m^2 g^{-1}$ even after calcination at 1373 K.

4. Conclusions

The HT-like materials prepared in the present study show an increase in the Mg/Al ratio and a decrease in the water content as the hydrothermal treatment is prolonged. Such a hydrothermal treatment leads to a sharp sintering of the solid from 115 $m^2 g^{-1}$ for the untreated samples to ca. 20 $m^2 g^{-1}$ after treatment for 8 days. Thermal decomposition takes place in three steps: the first corresponds to elimination of water molecules from the interlayer space, and, tentatively, the second step corresponds to elimination of carbonate anions, while the third step is due to elimination of hydroxyl groups from the brucite-like layers. Amorphous materials are then obtained, which crystallize upon calcination at temperatures close to 1000 K to yield MgO and $MgAl_2O_4$. These changes take place with a development of the specific surface area and a further sintering upon calcination above 1000 K.

Acknowledgements

The authors thank Dr M. J. Holgado and Mr A. Montero (Universidad de Salamanca) for assistance in obtaining some of the experimental data.

References

1. W. FEITKNECHT, *Helv. Chim. Acta* **25** (1942) 131.
2. W. FEITKNECHT and G. FISCHER, *ibid.* **18** (1935) 555.
3. W. T. REICHLE, *Solid State Ionics* **22** (1986) 135.
4. G. LAGALY, *ibid.* **22** (1986) 43.
5. S. MIYATA and T. HIROSE, *Clays & Clay Min.* **26** (1978) 441.

6. E. C. KRUISSINK, L. L. van REIJDEN and J. R. H. ROSS, *JCS Faraday I* **77** (1981) 649.
7. L. E. ALMAZORA, J. R. H. ROSS, E. C. KRUISSINK and L. L. van REIJDEN, *ibid.* **77** (1981) 665.
8. T. NAKATSUKA, H. KAWASAKI, S. YAMASHITA and S. KOKJIYA, *Bull. Chem. Soc. Jpn* **52** (1979) 244.
9. W. T. REICHLE, *J. Catal.* **94** (1985) 547.
10. R. SPINICCI and A. ULIBARRI, *Mater. Chem. Phys.* **26** (1990) 1.
11. W. SUZUKI, M. OKAMOTO and Y. ONO, *Chem. Lett.* (1989) 1485.
12. *Idem., ibid.* (1989) 1487.
13. H. KOPKA, K. BENEKE and G. LAGALY, *J. Colloid Interf. Sci.* **123** (1988) 427.
14. K. CHIBWE and W. JONES, *JCS Chem. Commun.* (1989) 926.
15. T. KWON, A. TSIGDINOS and T. J. PINNAVAIA, *J. Amer. Chem. Soc.* **110** (1988) 3653.
16. G. W. BRINDLEY and S. KIKKAWA, *Amer. Mineral.* **64** (1979) 836.
17. M. J. HERNANDEZ-MORENO, M. A. ULIBARRI, J. L. RENDON and C. J. SERNA, *Phys. Chem. Minerals* **12** (1985) 34.
18. K. NAKAMOTO, "Infrared and Raman Spectra of Inorganic and Coordination Compounds", 4th Edn (Wiley, New York, 1986) p. 121.
19. R. A. NYQUIST and R. O. KAGEL, "Infrared Spectra of Inorganic Compounds" (Academic, New York, 1971) pp. 206–207.
20. D. L. BISH and G. W. BRINDLEY, *Amer. Mineral.* **62** (1977) 458.
21. K. S. W. SING, D. H. EVERETT, R. A. W. HAUL, L. MOSCOU, R. PIEROTTI, J. ROUQUEROL and T. SIEMINIEWSKA, *Pure Appl. Chem.* **57** (1985) 603.

Received 14 November 1990
and accepted 10 April 1991